





Original Article



Centromere Protein I, a Cell Cycle Checkpoint Gene, Accelerates Tumor Progression via the Hippo Pathway and Mediates Immune Escape in Hepatocellular Carcinoma

Risheng He^{1,2#}, Yi Xu^{2,3,4,5#}, Pengbo Zhang⁶, Liang Yu², Jian Ma^{2,7*}  and Yunfu Cui^{2*} 

¹Department of Hepatobiliary and Pancreatic Surgery, The First People's Hospital of Yunnan Province; The Affiliated Hospital of Kunming University of Science and Technology, Kunming, Yunnan, China; ²Department of Pancreatobiliary Surgery, The Second Affiliated Hospital of Harbin Medical University, Harbin, Heilongjiang, China; ³State Key Laboratory of Oncology in South China, Cancer Center of Sun Yat-sen University, Guangzhou, Guangdong, China; ⁴Department of Pathology, Li Ka Shing Faculty of Medicine, The University of Hong Kong, Hong Kong, China; ⁵Shanghai Key Laboratory of Cancer Systems Regulation and Clinical, Shanghai, China; ⁶Department of Gastrointestinal Surgery, the People's Hospital of Zhaoyuan City, Zhaoyuan, Shandong, China; ⁷Department of Immunology, Harbin Medical University, Harbin, Heilongjiang, China

Received: March 19, 2025 | Revised: July 29, 2025 | Accepted: September 02, 2025 | Published online: September 24, 2025

Abstract

Background and Aims: Cell cycle checkpoint-related genes (CCCRGs) are implicated in the development and progression of hepatocellular carcinoma (HCC). However, their precise roles and underlying mechanisms remain insufficiently characterized and require further investigation. This study aimed to explore the prognostic significance of CCCRGs in HCC, and to investigate the mechanism by which they promote the progression of HCC. **Methods:** HCC datasets from The Cancer Genome Atlas and International Cancer Genome Consortium were analyzed to identify hub genes. A prognostic model was constructed and validated using Kaplan-Meier analysis, nomogram, calibration curves, decision curve analysis, and receiver operating characteristic analysis. Immune infiltration patterns were assessed using single sample gene set enrichment analysis, while pathway activities were evaluated via gene set variation analysis. Single-cell RNA sequencing data from GSE149614 were analyzed with Seurat and CellChat to investigate cell-cell communication. Patient-derived HCC specimens were examined through immunohistological evaluation, HCC cell lines were used for *in vitro* functional assays, and *in vivo* tumor growth was assessed through animal experiments. **Results:** CCCRGs showed significant associations with prognosis, malignant biological behavior, and immune responses in HCC. Centromere protein (CENP) I was identified as a critical hub gene that markedly promoted HCC proliferation, metastasis, and epithelial-mesenchymal transition, while inhibiting apoptosis. Mechanistically, CENPI suppressed YAP phosphorylation, enhancing its

nuclear translocation and thereby driving malignant progression. Additionally, CENPI impaired immune effector cell infiltration, likely by disrupting tumor antigen presentation and chemokine-mediated CD8⁺ T cell chemotaxis, thereby promoting immune escape. **Conclusions:** This study underscores the prognostic significance of CCCRGs in HCC and identifies CENPI as a key driver of tumor progression through the Hippo pathway. Furthermore, it reveals CENPI's role in promoting immune escape, suggesting novel therapeutic targets for HCC treatment.

Citation of this article: He R, Xu Y, Zhang P, Yu L, Ma J, Cui Y. Centromere Protein I, a Cell Cycle Checkpoint Gene, Accelerates Tumor Progression via the Hippo Pathway and Mediates Immune Escape in Hepatocellular Carcinoma. J Clin Transl Hepatol 2025. doi: 10.14218/JCTH.2025.00127.

Introduction

Hepatocellular carcinoma (HCC) accounts for roughly 90% of primary liver cancers and ranks among the most lethal malignancies, with the fourth-highest cancer-related mortality rate globally.¹ Its primary causes include viral hepatitis, alcohol-induced cirrhosis, and fatty liver disease, among others.² Despite notable advances in treatment modalities in recent years, the five-year overall survival (OS) rate for HCC patients remains disappointingly low, with only 5% to 15% of early-stage cases qualifying for surgical resection.³ Even after surgery, patients face a substantial risk of recurrence. Due to HCC's insidious onset and rapid progression, it is often diagnosed at advanced stages. Currently, more than 90% of HCC patients receive treatments such as chemotherapy, immunotherapy, transarterial chemoembolization, and tyrosine kinase inhibitors.^{4,5} However, the clinical effectiveness of these therapies remains suboptimal. Effectively curbing tumor growth and preventing metastasis continue to be formidable challenges. Furthermore, the heterogeneity of HCC

Keywords: Hepatocellular carcinoma; Cell cycle checkpoint; Hub gene; Prognostic model; Malignant biological behavior; Immune escape.

*Contributed equally to this work.

Correspondence to: Yunfu Cui and Jian Ma, Department of Pancreatobiliary Surgery, The Second Affiliated Hospital of Harbin Medical University, Harbin, Heilongjiang 150086, China. ORCID: <https://orcid.org/0000-0001-7393-1680> (YC) and <https://orcid.org/0000-0001-8223-8327> (JM). Tel: +86-451-86605113, Fax: +86-451-86605356, E-mail: yfcui7@163.com (YC) and jma@hrbmu.edu.cn (JM).

complicates prognosis prediction and clinical decision-making. Therefore, there is an urgent need to identify new and reliable screening methods to improve diagnostic accuracy, better predict patient outcomes, and provide a foundation for personalized treatment strategies.

Cell proliferation is tightly regulated by a series of conserved cell cycle control mechanisms to ensure the generation of two genetically identical daughter cells.⁶ Cell cycle checkpoints (CCCs) serve as guardians of DNA integrity, preventing the accumulation and propagation of genetic errors during division. These checkpoints can arrest cell cycle progression or, in cases of irreparable DNA damage, trigger cell cycle exit or apoptosis.⁷ Cancer is characterized by uncontrolled cellular hyperproliferation, with CCC dysfunction playing a pivotal role in its pathogenesis.⁸ CHK1, a DNA damage checkpoint kinase, is crucial for regulating DNA replication, phase transitions, and mitotic events. Elevated CHK1 expression is significantly associated with clinical outcomes, including prognosis, relapse rates, and drug resistance across various malignancies.⁹ Centromere proteins (CENPs) are essential for mitosis, participating in centromere formation and chromosome segregation. Previous studies have reported a notable increase in CENPA levels in HCC, correlating with disease progression by upregulating cyclin D1 and neuropilin 2 through YY1 transcriptional activation and collaboration with YY1.¹⁰ While the roles of certain cell cycle checkpoint-related genes (CCCRGs) in HCC progression have been extensively studied, most research has focused on individual genes. However, the prognostic significance of the collective transcriptional profile of CCCRGs in HCC remains inadequately explored. Moreover, the functional contributions of many CCCRGs in HCC warrant further investigation.

The tumor immune landscape reflects a complex interplay among tumor cells, diverse immune cell subsets, and the cytokines they secrete. Immune cells can be broadly categorized by function into pro-inflammatory cells, such as effector CD8⁺ T cells and natural killer (NK) cells, and immunosuppressive cells, including M2 macrophages, regulatory T cells, and myeloid-derived suppressor cells. Tumors employ multiple mechanisms to modulate immune cell infiltration and depletion, while reciprocal interactions also occur among these immune cells.¹¹ Recent advances in HCC immunotherapy have shown that while immune checkpoint inhibitors elicit strong antitumor responses in certain patient populations, combination therapies incorporating immune checkpoint inhibitors with other agents generally achieve superior outcomes. Notably, the atezolizumab–bevacizumab combination has become a first-line treatment for HCC. Conversely, other immunotherapeutic strategies, including adoptive T-cell therapy, cancer vaccines, and oncolytic virotherapy, have demonstrated limited and inconsistent clinical efficacy to date.¹¹ Furthermore, the reconfiguration of the immune microenvironment in HCC has drawn increasing attention. For instance, one study revealed that interactions between SPP1-positive macrophages and cancer-associated fibroblasts form a tumor immune barrier within HCC, which impedes CD8⁺ T-cell infiltration into the tumor core and significantly diminishes the therapeutic efficacy of immunotherapy.¹² Despite extensive research on immune microenvironment reconfiguration in HCC, the role of CCCRGs in this process remains poorly understood.

In this study, we employed a robust bioinformatics strategy, incorporating weighted gene co-expression network analysis (WGCNA) and related methods,¹³ to identify 22 CCCRGs significantly associated with poor prognosis in HCC. These key genes were then employed to construct a

prognostic risk model aimed at enhancing clinicians' ability to predict patient survival and therapeutic responses with greater accuracy. Among these, CENPI emerged as a critical target gene, yet its functional role and underlying mechanisms in HCC progression remained unclear. Subsequent experimental investigations demonstrated that CENPI promotes HCC cell proliferation, migration, and invasion by modulating the Hippo signaling pathway and regulating epithelial-mesenchymal transition (EMT). Importantly, our findings underscore CENPI's role in reshaping the tumor immune microenvironment (TIME) and suppressing the infiltration of pro-inflammatory immune cells, including CD8⁺ T lymphocytes and NK cells. These findings suggest that CENPI represents a promising therapeutic target for HCC management.

Methods

Bioinformatics processing and analysis

High-quality HCC gene expression datasets were selected from The Cancer Genome Atlas (TCGA) and International Cancer Genome Consortium (ICGC) databases according to strict inclusion criteria. Samples were excluded if they had incomplete follow-up data, missing survival information, survival durations under 30 days, or redundant sequencing from the same patient. Ultimately, 343 tumor samples from the TCGA-Liver Hepatocellular Carcinoma (LIHC) dataset and 226 from the ICGC-Liver Cancer-Riken-Japan (LIRI-JP) dataset were included. A list of 292 CCCRGs was also obtained from pathcards.genecards.org. Employing WGCNA and differential expression analysis, we identified genes strongly correlated with tumorigenesis and poor prognosis, and cross-referenced these with the CCCRG list to pinpoint key genes.¹³ Lasso regression and Random Forest (RF) algorithms were applied to further refine and isolate hub genes.^{14,15} TCGA HCC tumor samples were designated as the training set, while ICGC-LIRI-JP samples served as the validation set. A prognostic model incorporating these hub genes was constructed using the training set and validated with the validation set. Kaplan–Meier curves were generated to evaluate OS across different groups.¹⁶ Nomograms and calibration curves were constructed to assess the model's predictive accuracy for survival probabilities.¹⁷ Decision curve analysis was conducted to evaluate the clinical utility of the model, and receiver operating characteristic (ROC) curves were plotted to assess its predictive performance for postoperative survival.¹⁸ Gene set enrichment analysis and gene set variation analysis were employed to explore relevant pathways.¹⁹ The ESTIMATE algorithm was used to evaluate and compare stromal and immune scores between groups,²⁰ while single sample gene set enrichment analysis was applied to assess variations in immune cell infiltration patterns.²¹ The maftools package was utilized to visualize mutational landscapes of different risk cohorts.²²

The GSE149614 single-cell RNA sequencing dataset included tissue samples from 10 HCC patients, encompassing primary tumors, portal vein tumor thrombi, metastatic lymph nodes, and healthy liver tissues.²³ Using the "Seurat" package in R software, 10x single-cell RNA sequencing data were converted into Seurat objects. Raw counts underwent rigorous quality control (QC) to exclude low-quality cells, retaining only those with gene counts between 500 and 5000 and mitochondrial gene expression below 10%. Following the standard Seurat workflow, the data were normalized, subjected to principal component analysis, and batch effects were corrected using Harmony. Clustering was performed at

an optimal resolution determined via UMAP visualization, and cell subtypes were identified based on unique molecular expression profiles. The CellChat package was then used for a detailed analysis of cell–cell communication.²⁴

Specimens from patients

Liver tissue samples (n = 30) were collected from HCC patients after treatment, along with an equal number of matched non-neoplastic tissue controls, at the Second Affiliated Hospital of Harbin Medical University (Harbin, China). The study protocol was approved by the hospital's Ethics Committee, and all participants provided written informed consent (YJSKY2023-148).

Cell culture

Human HCC cell lines and normal liver cells were obtained from Zhongqiao Xinzhou Biotechnology Co., Ltd. (Shanghai, China). Cells were cultured in Dulbecco's modified Eagle medium supplemented with 10% fetal bovine serum (FBS) and 1% penicillin–streptomycin (Beyotime, Shanghai, China) at 37°C in a 5% CO₂ incubator.²⁵

Gene knockdown

For CENPI knockdown, shRNA and negative control (shNC) sequences were designed as follows: shCENPI-1: GCTCTCTTTACATCAACCAT, shCENPI-2: CTGCTCTGATTTTCAGTATCTT, shCENPI-3: CTGAAAGAGCTATTGCAGAAT, shCENPI-4: AGGCTTTGTTGTCACTGTATA, shCENPI-5: TTGCAAATGGCAGTGGGATAT, shNC: TTCTCCGAACGTGTACAGT.²⁶

Western blot analysis

Proteins were extracted from tissue and cellular samples using RIPA buffer (Beyotime, Shanghai, China) supplemented with protease and phosphatase inhibitors (Roche, Switzerland). Protein concentration was determined with a bicinchoninic acid assay kit (Beyotime, Shanghai, China). Proteins were separated by SDS–PAGE, transferred to nitrocellulose membranes, and blocked according to standard protocols. Membranes were incubated overnight at 4°C with the following primary antibodies: β -actin (#8480, CST, 1:1000), CENPI (ab118796, Abcam, 1:1,000), E-cadherin (TA0131, Abmart, 1:1,000), N-cadherin (T55015, Abmart, 1:1,000), Vimentin (#5741, CST, 1:1,000), YAP1 (T55381, Abmart, 1:5,000), and phospho-YAP1 (T55743, Abmart, 1:5,000). After three washes with TBST buffer, membranes were incubated with diluted secondary antibodies for 1 h, washed again, and then exposed to ECL developing solution. After a two-minute incubation in the dark, membranes were imaged using an automated chemiluminescence imaging system.²⁷

CCK-8

Cells were harvested, centrifuged, and resuspended in complete culture medium for counting. Subsequently, 5×10^3 cells in 100 μ L of medium were seeded into each well of a 96-well plate and incubated for 24, 48, and 72 h. At each time point, 10 μ L of CCK-8 solution (Beyotime, Shanghai, China) was added to each well, followed by a 2-h incubation. The optical density at 450 nm was measured and recorded for each well.²⁸

EdU

Cells were cultured in 6-well plates until adherent, then incubated with 2 mL of 1 \times EdU working solution for 2 h. Following incubation, cells were washed, fixed with 4% paraformaldehyde, and permeabilized with PBS containing 0.3%

Triton X-100. They were then incubated with a Click reaction mixture for 30 m in the dark, stained with 1 \times Hoechst 33342 to visualize nuclei, and examined using a confocal laser scanning microscope.²⁹

Colony formation assay

When cells in each group reached the desired density, they were harvested and centrifuged. A total of 1,000 cells per well were seeded into 6-well plates and cultured continuously for 12 days. Colonies were then fixed with 4% paraformaldehyde for 30 m and stained with 1% crystal violet for 20 m. The number of colonies was subsequently counted and recorded.³⁰

Wound healing assay

After transfection, cells were grown in 6-well plates until they reached confluence. A scratch was made across the monolayer using a 200 μ L pipette tip, and non-adherent cells were removed by washing with PBS. The initial wound edge (0-h time point) was imaged at 40 \times magnification. Cells were then incubated in serum-free medium, and wound closure was monitored and photographed at 24 and 48 h using a 40 \times microscope.³¹

Transwell assay

For the invasion assay, the upper chamber of the transwell insert was coated with approximately 50 μ L of Matrigel and allowed to solidify. Cells were resuspended in serum-free medium, and 200 μ L of the suspension was added to the upper chamber. The lower chamber was filled with 800 μ L of Dulbecco's modified Eagle medium containing 10% fetal bovine serum. After 24 and 48 h of incubation, invasive cells that had migrated to the lower chamber were fixed with methanol and stained with 1% crystal violet. Cell invasion was then assessed and photographed under a microscope at 100 \times magnification.³²

Flow cytometry

Apoptosis was evaluated using the Annexin V–FITC/PI Apoptosis Kit (BD, USA). Cells were harvested at the desired density, centrifuged, and washed with pre-chilled PBS. After counting, an appropriate volume of the suspension was re-centrifuged, and the supernatant was discarded. The cell pellet was resuspended in 100 μ L of binding buffer and transferred into flow cytometry tubes. Cells were then stained with Annexin V–FITC and PI, followed by 15 m of incubation at room temperature in the dark. After incubation, 400 μ L of binding buffer was added, and apoptosis was analyzed by flow cytometry.³³

Immunofluorescence

Cells were seeded at optimal density in 24-well plates and allowed to adhere. After fixation with 4% paraformaldehyde, cells were permeabilized and blocked. The primary antibody against YAP was incubated with the cells overnight at 4°C. The following day, a fluorescent secondary antibody was applied, and nuclei were counterstained with DAPI. Stained cells were visualized under a fluorescence inverted microscope.³⁴

Formalin-fixed, paraffin-embedded tissue specimens were sectioned at 4 μ m. After dewaxing with xylene and rehydration through graded ethanol, antigen retrieval was performed using 0.1 M citrate buffer (pH 6.0) with heat-induced epitope recovery. Sections were incubated overnight at 4 °C with primary antibodies against CD3 (ZM-0417) and CD8 (ZA-0508), followed by incubation with fluorescently conjugated secondary antibodies at 37°C for 60 m. Nuclei were coun-

Table 1. The sequences of primers

Genes	Forward primer (5'-3')	Reverse primer (5'-3')
GAPDH	ACCGGGAAGGAAATGAATGG	CCCAATACGACCAAATCAGAGA
B2M	AAAGATGAGTATGCCTGCCG	CGGCATCTTCAAACCTCCAT
CXCL9	CCAATACAGGAGTGACTTGGA	CTCACTACTGGGGTTCCTTG
CXCL10	AGTGGCATTCAAGGAGTACC	ACGTGGACAAAATTGGCTTG
CXCL11	ACAGTTGTTCAAGGCTTCCC	CTTGCTTGCTTCGATTGGG

terstained with DAPI, and fluorescence was quantified using epifluorescence microscopy.³⁵

Animal experiments

Once cells reached confluence, they were harvested, centrifuged, and resuspended in pre-chilled PBS for counting. A total of 5×10^6 Hep3B cells were resuspended in 200 μ L of pre-chilled PBS and implanted subcutaneously into the axillae of six-week-old male nude mice. Mice were housed under standard conditions with free access to food and water and maintained on a 12-h light/dark cycle. Tumor size was measured every three days starting on day 6 post-implantation. After three weeks, mice were euthanized, and tumors were excised, weighed, and recorded for analysis.³⁶ All animal experiments were approved by the Ethics Committee of the Second Affiliated Hospital of Harbin Medical University (YJS-DW2023-067).

Quantitative reverse transcription polymerase chain reaction analysis

Total RNA was extracted from Hep3B cells using TRIzol reagent (Invitrogen) and reverse-transcribed into cDNA with the Transcriptor First Strand cDNA Synthesis Kit (Roche, Penzberg, Germany). FastStart Universal SYBR Green Master (Roche) was used to amplify each sample in a 20 μ L reaction mixture. The fold changes were converted using the $2^{-\Delta\Delta C_t}$ technique. Expression levels were determined by calculating and normalizing them to the endogenous GAPDH.³⁷ The primer sequences are listed in Table 1.

Statistical analysis

Data are presented as mean \pm standard deviation from at least three independent experiments. Statistical differences between two groups were analyzed using an independent-samples t-test, while one-way ANOVA was used for comparisons among multiple groups. Analyses were performed with GraphPad Prism 8.0 and R version 4.2.3. Statistical significance was defined as $p < 0.05$.

Results

Weighted gene co-expression network construction

We analyzed normal and tumor samples from the TCGA-LIHC cohort to identify regulatory genes involved in HCC initiation. To delineate densely connected gene clusters within the microarray samples, correlation network analyses were performed. WGCNA was used to construct and systematically analyze active tumor-related networks. Following sample clustering, an appropriate threshold ($\text{cutHeight} = 210$) was applied to remove samples exhibiting conspicuous anomalies, as illustrated in Figure 1A. After outlier removal, a sample clustering dendrogram was constructed (Fig. 1B). For subsequent analyses, the top 8,000 genes were selected. An

adjacency matrix was generated using a soft-threshold power of $\beta = 8$ ($R^2 = 0.85$), ensuring a scale-free network topology for gene distribution, as depicted in Figure 1C, thereby preserving crucial connectivity information. Using parameters of $\text{minModuleSize} = 30$ and $\text{mergeCutHeight} = 0.25$, we identified 12 distinct modules (Fig. 1D). Module connectivity was calculated, and clustering analysis incorporating grouping information yielded a heatmap (Fig. 1E). To explore module-phenotype associations, we computed correlation coefficients between each module and tumor traits, revealing six modules with statistically significant links to HCC. Notably, the "blue" ($r = 0.63$, $p = 4e-48$) and "turquoise" ($r = 0.55$, $p = 3e-34$) modules showed the strongest correlations with tumor status (Fig. 1F). We then performed module membership and gene significance correlation analyses on these two modules, observing a strong positive correlation between module membership and gene significance (Fig. 1G). By merging gene sets from both modules, we compiled a final subset of 3826 module-associated genes for further investigation.

The identification of hub CCRGs implicated in HCC development and associated with unfavorable prognoses

Differential expression analysis was performed to compare gene expression profiles between normal and tumor samples from the TCGA-LIHC dataset. Gene expression fold changes (FCs) were transformed to log2 scale, and a stringent cutoff of $|\log_2\text{FC}| \geq 2$ with $p < 0.05$ was applied to identify differentially expressed genes. Under these criteria, 1,159 genes were identified as potentially involved in tumor progression, including 471 upregulated and 688 downregulated genes (Fig. 2A). Upregulated genes were prioritized for subsequent investigation. Similarly, differential expression analysis of tumor samples stratified by clinical stage was conducted, applying thresholds of $|\log_2\text{FC}| \geq 0.2$ and $p < 0.05$. This yielded 918 stage-associated genes, including 387 upregulated and 531 downregulated genes (Fig. 2B), with upregulated genes selected for further analysis. To identify genes significantly influencing postoperative OS, survival analysis was performed on tumor samples, retaining genes with $p < 0.01$. Through integrative analysis of differentially expressed genes, module genes, and CCRGs, 29 key genes were identified (Fig. 2C). LASSO Cox regression analysis was then employed to select the most informative diagnostic features, identifying 26 candidates (Fig. 2D and E). The RF algorithm was subsequently applied to rank gene importance, generating a list of 29 genes. The top 25 genes with the highest importance scores were selected for further investigation (Fig. 2F). By intersecting results from LASSO Cox regression and RF analyses, 22 optimal gene signatures were identified and defined as hub genes (Fig. 2G). Box plots illustrated differential expression of these hub genes between normal and tumor samples (Fig. 2H). ROC curve analysis

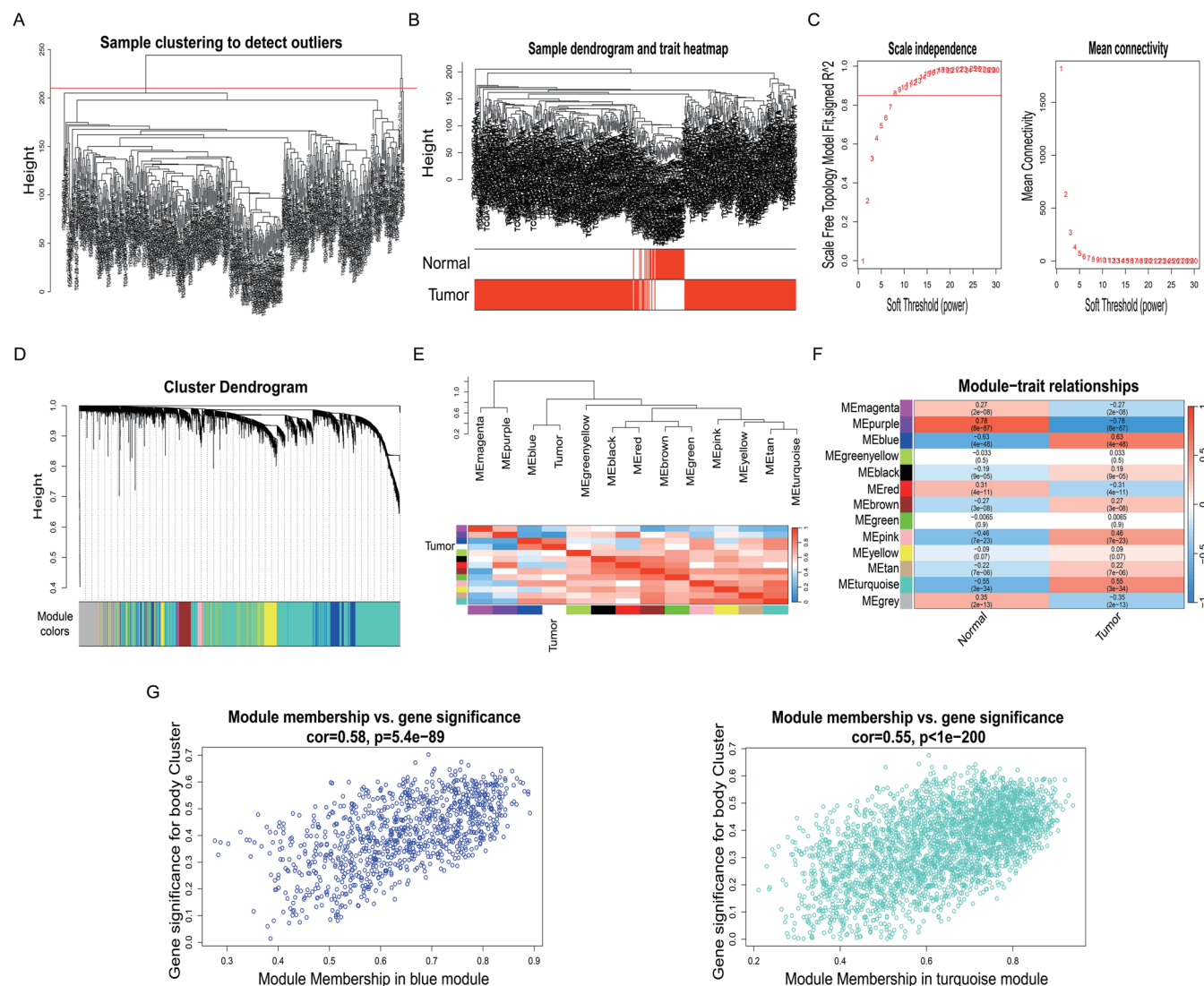


Fig. 1. Detection of module genes using WGCNA. (A) Sample clustering with exclusion of outliers. (B) The expression matrix was clustered, with color coding indicative of disease status (normal versus tumor). (C) A “soft” threshold was selected. (D) Cluster dendrogram. (E) A heat map of module eigengenes. (F) The interplay between modules and traits. (G) A scatter diagram of MM versus GS. GS, Gene significance; MM, Module membership; WGCNA, Weighted gene co-expression network analysis.

demonstrated robust diagnostic performance (Supplementary Fig. 1). Correlation analysis revealed potential interactions among most hub genes (Fig. 2I), suggesting coordinated regulatory roles in tumor progression.

Comprehensive analysis of the risk score in HCC patients in conjunction with clinical parameters

We employed the TCGA-LIHC dataset as the training cohort to develop a predictive model by integrating hub gene expression profiles with patient survival data, while the ICGC-LIRI-JP dataset was utilized for external validation. Initially, the optimal cutoff point was determined within the training set (Fig. 3A). Based on this threshold, patients were stratified into high-risk and low-risk subgroups. Patients above the cutoff point exhibited significantly higher risk scores, lower survival rates, and elevated expression of hub genes (Fig. 3B). Cox regression analysis revealed a hazard ratio of 2.53 for the risk score (95% CI: 1.98–3.2; $p < 0.001$), surpass-

ing the prognostic value of clinical factors such as age, gender, and stage (hazard ratio = 1.55; 95% CI: 1.24–1.9; $p < 0.001$), indicating the risk score’s robustness as a prognostic indicator (Fig. 3C). Kaplan–Meier analysis showed significantly reduced OS in the high-risk group ($p < 0.0001$), with very few survivors beyond five years (Fig. 3D). Similar results were obtained in the validation cohort (Supplementary Fig. 2A–D). To further refine prognostic prediction, we integrated the risk score with clinical factors (age, gender, and stage) to construct a nomogram (Fig. 3E). The calibration plot demonstrated strong agreement between nomogram-predicted and observed one-, three-, and five-year OS, confirming its reliability (Fig. 3F). ROC curve analysis further validated the predictive accuracy of the risk score for one-, three-, and five-year OS (Fig. 3G). Decision curve analysis emphasized the clinical utility of the risk score in guiding treatment decisions (Fig. 3H). As most patients in the validation cohort had OS between one and three years, we assessed time points at

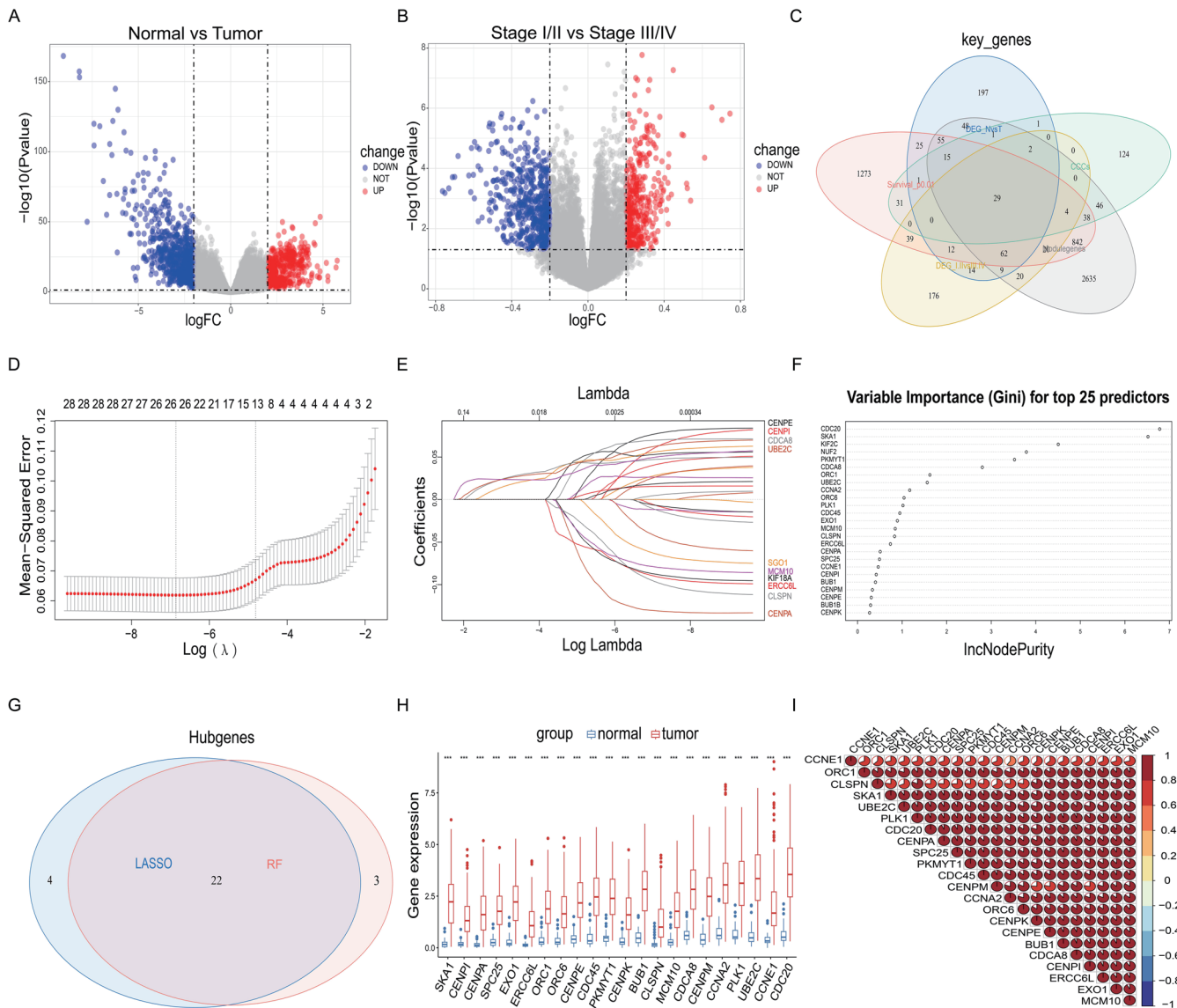


Fig. 2. Identification of hub genes associated with CCCs. (A) Volcano plot comparing DEGs between the normal and tumor groups. (B) Volcano plot comparing DEGs between the I/II and III/IV groups. (C) The Venn diagram showing key genes. (D, E) LASSO regression analysis. (F) RF algorithm. (G) The Venn diagram showing the hub genes. (H) Differences in expression levels of 22 hub genes. (I) Correlation among the 22 hub genes. *** $p < 0.001$. CCCs, Cell cycle checkpoints; DEGs, Differentially expressed genes; LASSO, Least absolute shrinkage and selection operator; RF, Random forest.

one, two, and three years, achieving consistent results (Supplementary Fig. 2E–H).

Analysis of immune cell infiltration and genetic mutation landscapes in model-delineated high- and low-risk groups

Using the ESTIMATE algorithm, we analyzed the infiltration levels of immune and stromal cell populations within the tumor microenvironment. As shown in Figure 4A–C, high-risk patients exhibited a significant reduction in stromal scores compared to their low-risk counterparts, while no notable differences were observed in immune scores or ESTIMATE scores between the two groups. Although these findings suggested comparable overall immune scores, they did not accurately reflect the infiltration status of individual immune cell subsets. To address this limitation, we utilized single

sample gene set enrichment analysis to quantify the distribution of 28 immune cell subsets within tumor tissues from high- and low-risk cohorts (Fig. 4D). Notably, the high-risk group demonstrated elevated infiltration of type 2 T helper cells, NK T cells, effector memory CD4⁺ T cells, and activated CD4⁺ T cells. Conversely, monocytes, central memory CD4⁺ T cells, CD56dim NK cells, plasmacytoid dendritic cells (DCs), NK cells, effector memory CD8⁺ T cells, type 1 T helper cells, and eosinophils were more abundant in the low-risk group. Furthermore, a comparative analysis of immune cell exhaustion marker expression revealed significant upregulation in the high-risk cohort (Fig. 4E). We then conducted an in-depth analysis of genetic mutation profiles in the high- and low-risk groups, identifying the top 10 genes with the highest mutation frequencies. CTNNB1 exhibited the highest mutation frequency in the low-risk group (29%), while TP53

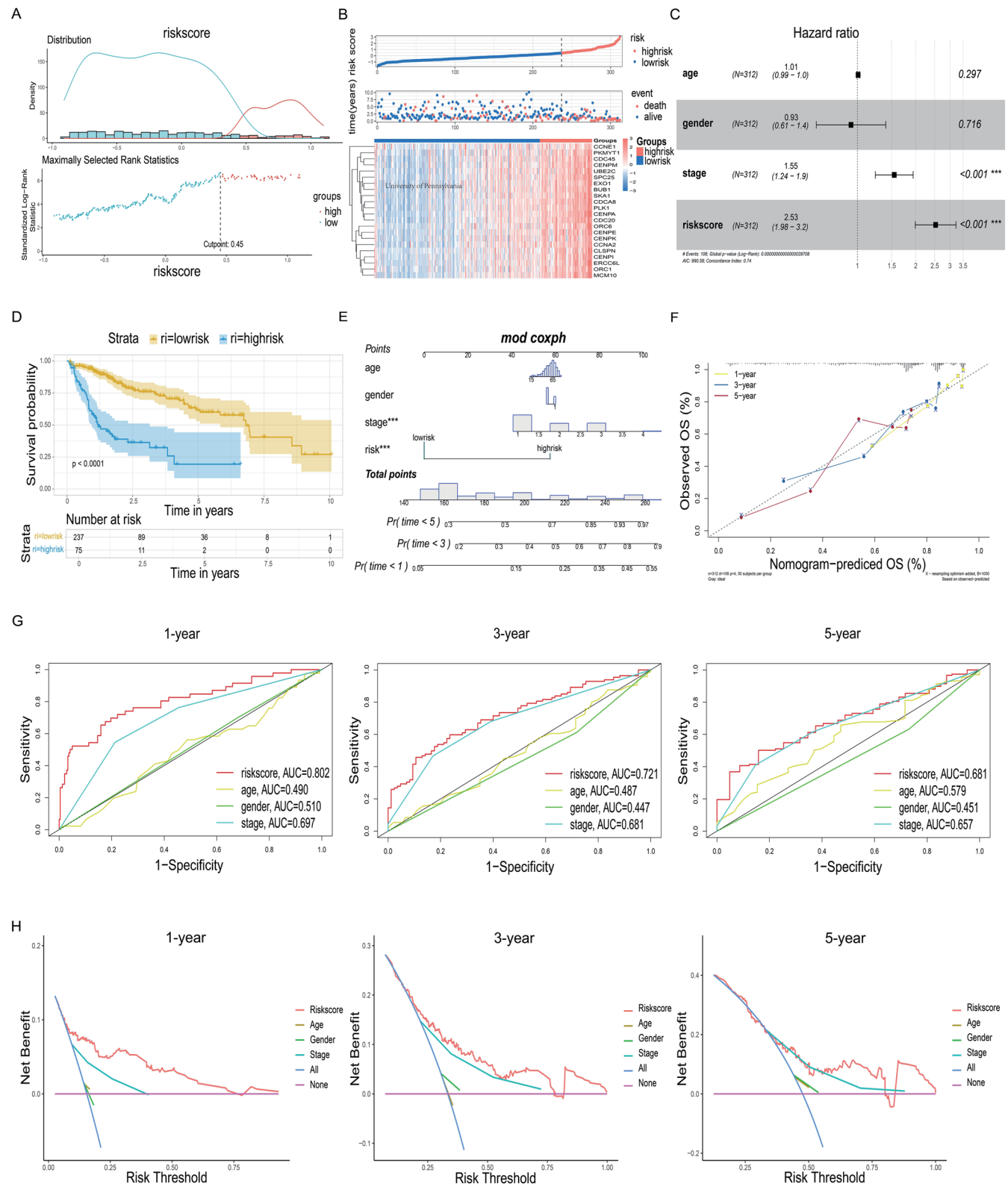


Fig. 3. Construction and evaluation of a risk scoring model in the training set. (A) The optimal cutoff point calculated within the training set. (B) A dot plot of the risk score distribution, a scatter plot of patient survival status, and a heat map of the model's gene expression. (C) Cox regression analysis. (D) Survival analysis. (E) A nomogram. (F) A calibration curve for the nomogram. (G) ROC curves for one-, three-, and five-year OS. (H) DCA for one, three, and five years. *** $p < 0.001$. AUC, Area under curve; DCA, Decision curve analysis; OS, Overall survival; ROC, Receiver operating characteristic.

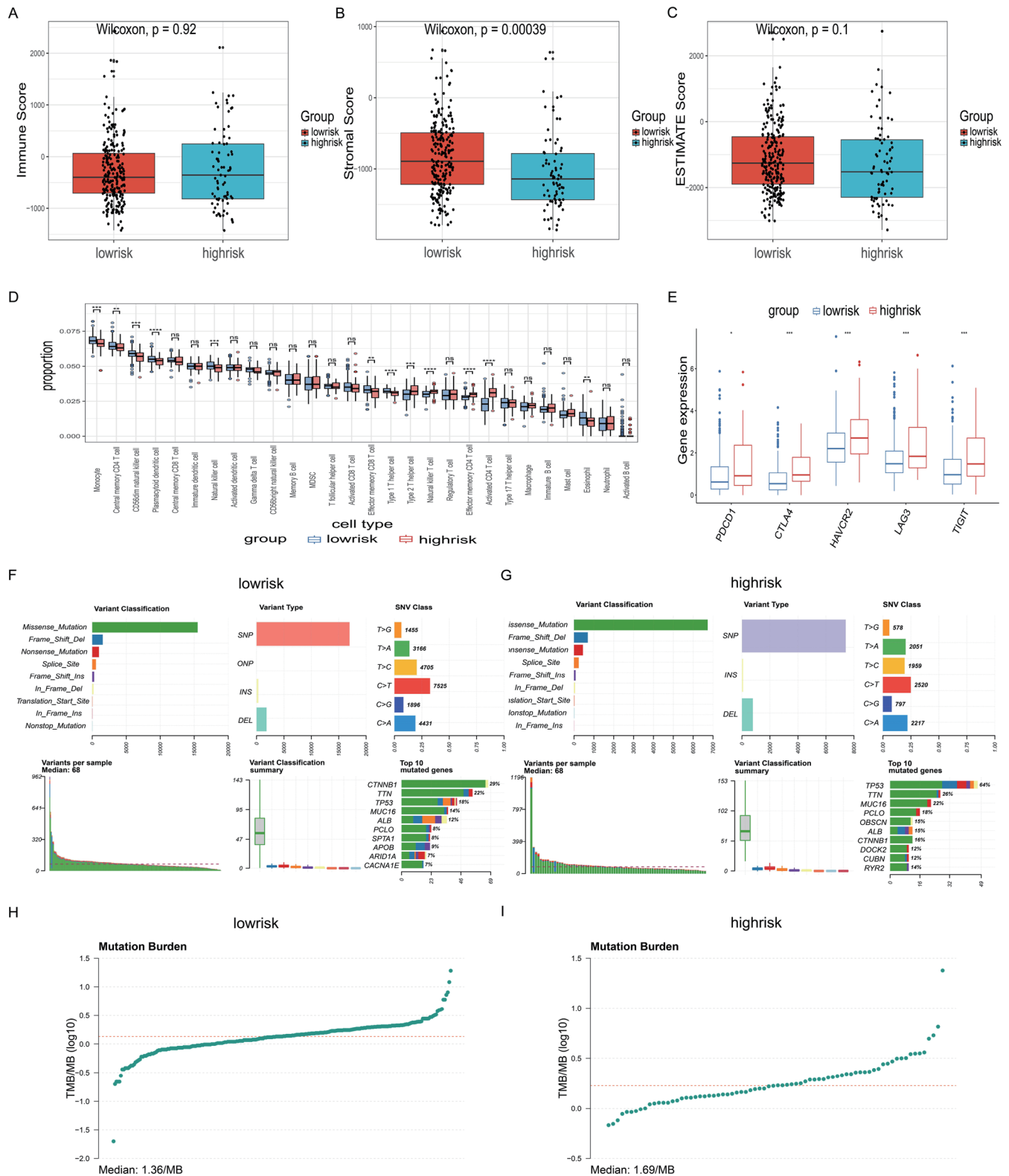


Fig. 4. Immune cell infiltration and gene mutation analysis of high- and low-risk groups. (A) Immune score assessment. (B) Stromal score evaluation. (C) ESTIMATE score analysis. (D) Infiltration levels of 28 immune cell subtypes in high- and low-risk groups. (E) Levels of immune cell exhaustion markers in high- and low-risk groups. (F, G) Somatic mutation characteristics in the two groups. (H, I) TMB analysis in the two groups. * $p < 0.05$; ** $p < 0.01$; *** $p < 0.001$; **** $p < 0.0001$. MB, Megabase; MDSC, Myeloid-derived suppressor cell; TMB, Tumor mutation burden.

was the most frequently mutated gene in the high-risk group (64%) (Fig. 4F and G). Finally, tumor mutation burden analysis revealed a significantly higher tumor mutation burden in the high-risk group compared to the low-risk group (Fig. 4H and I).

CENPI was overexpressed in HCC tissues and cell lines and associated with poor prognosis

Among the 22 previously identified hub genes, the expression pattern and functional role of CENPI in HCC remain inadequately characterized, with limited validation and mechanistic insights into its contribution to disease progression. To address this gap, we focused our subsequent investigations on CENPI. Initially, we observed significant overexpression of CENPI in tumor samples from the TCGA-LIHC dataset (Fig. 2H). To further elucidate its expression pattern in patient tissues, we analyzed the single-cell sequencing dataset GSE149614. Using PC = 30 for dimensionality reduction via UMAP, followed by clustering at a resolution of 2, we identified 55 distinct subgroups from cells that passed QC (Supplementary Fig. 3A and B). These clusters were annotated as "B cell", "CD4⁺ T cell", "CD8⁺ T cell", "DC", "endothelial cell", "fibroblast", "hepatocyte", "macrophage", "monocyte", and "NK cell" (Fig. 5A). Characteristic gene expression profiles for each cell type are presented in Supplementary Figure 3C and D. CENPI expression was predominantly detected in hepatocytes, with moderate levels in endothelial cells, DCs, and macrophages (Fig. 5B). To minimize the confounding effects of stromal cells, we extracted hepatocyte data for further analysis, which confirmed significantly elevated CENPI expression in tumor tissues compared to normal tissues across most samples. Interestingly, elevated CENPI expression was also observed in the metastatic lymph nodes and portal vein tumor thrombi of some patients, suggesting a potential role in distant metastasis (Fig. 5C). These bioinformatics findings were further validated *in vitro*, confirming upregulated CENPI expression in HCC tissues and cell lines (Fig. 5D). Using predefined expression thresholds, we evaluated the correlation between CENPI expression and TNM stage, revealing that high CENPI expression correlated with advanced disease (Fig. 5E). Moreover, survival analysis revealed that patients with elevated CENPI expression exhibited poorer OS (Fig. 5F and G). Gene set enrichment analysis demonstrated that CENPI overexpression was closely related to HCC proliferation, metastasis, and EMT (Fig. 5H).

CENPI facilitated HCC cell proliferation

To investigate the functional role of CENPI in tumor cell behavior, we selected Hep3B (TP53-null) and HCCLM3 (highly metastatic) cell lines for silencing experiments, given their relatively high endogenous CENPI expression. Efficient CENPI knockdown was achieved in both cell lines, as confirmed by experimental validation (Fig. 6A and B). The two clones with the strongest knockdown efficiency from each cell line were selected for subsequent experiments. A series of *in vitro* assays, including CCK-8 proliferation, EdU incorporation, and colony formation, consistently revealed that CENPI silencing significantly impaired proliferative capacity and clonogenic potential, consistent with the bioinformatics analyses (Fig. 6C–J). Furthermore, flow cytometry showed that CENPI knockdown induced apoptosis in HCC cells, supporting its pro-tumorigenic role (Fig. 6K–N). In an *in vivo* subcutaneous xenograft model, CENPI knockdown markedly suppressed tumor growth, as evidenced by significantly reduced tumor weight and volume compared to controls (Fig. 6O and P).

CENPI promoted HCC cell migration, invasion, and EMT

To assess the effects of CENPI knockdown on tumor cell motility and invasiveness, we performed wound healing and transwell assays. The wound healing assay revealed a significant reduction in migratory capacity in CENPI knockdown groups compared to controls (Fig. 7A–D). Similarly, transwell invasion assays demonstrated markedly reduced invasive potential, with fewer cells traversing the membrane in knockdown groups versus controls (Fig. 7E and F). Additionally, CENPI suppression significantly altered EMT marker expression, downregulating mesenchymal markers while upregulating epithelial markers, indicating impaired metastatic potential (Fig. 7G–J).

CENPI promoted the malignant biological behavior of HCC cells via the Hippo pathway

We investigated the molecular mechanisms underlying CENPI's role in HCC proliferation and metastasis. Gene set variation analysis of CENPI confirmed its significant enrichment in the Hippo pathway (Fig. 8A). The Hippo pathway played a pivotal role in regulating liver size, regeneration, stem cell self-renewal, and HCC progression.³⁸ Extensive previous research has demonstrated a close association between the Hippo pathway and HCC proliferation and metastasis.^{39,40} For example, reduced succinate dehydrogenase (SDH) activity has been linked to succinate accumulation and poor HCC prognosis, with SDHA and SDHB downregulation promoting HCC progression via the YAP1/TAZ oncogenic signaling axis through impaired proteasomal degradation pathways.⁴¹ In our study, CENPI knockdown significantly increased phosphorylated YAP levels while decreasing total YAP expression in HCC cells (Fig. 8B–E). Furthermore, CENPI suppression reduced nuclear localization of YAP (Fig. 8F and G). These findings suggest that CENPI regulates the Hippo signaling pathway by inhibiting YAP phosphorylation and facilitating its nuclear translocation, thereby promoting HCC cell proliferation and metastatic potential.

CENPI mediated immune escape in HCC patients

We analyzed the impact of CENPI on the TIME in HCC patients by extracting all tumor samples from the single-cell sequencing dataset GSE149614. Using PC = 30, we performed UMAP dimensionality reduction on cells passing QC and identified 62 subgroups at a resolution of 3 (Supplementary Fig. 4A and B). These 62 clusters were classified as "B cell", "CD4⁺ T cell", "CD8⁺ T cell", "DC", "endothelial cell", "fibroblast", "HCC", "macrophage", "monocyte", and "NK cell" (Fig. 9A). Characteristic gene expressions for each cell type are depicted in Supplementary Figure 4C and D. To exclude the influence of CENPI expression in other cell types, we extracted the HCC subset from the tumor samples and analyzed CENPI expression. Patients were classified into low- and high-CENPI expression groups based on their expression profiles (Fig. 9B). Figure 9C shows the proportion of different cell types in the two groups. A notable rise in the percentage of HCC cells was observed in the high-expression cohort, consistent with the finding that CENPI enhanced tumor proliferation. Furthermore, the low-expression group exhibited increased proportions of endothelial cells and fibroblasts. Notably, several immune cell types, including NK cells, DCs, and CD4⁺ T cells, were markedly reduced in the high-expression group. Multiparametric immune profiling revealed significant associations between CENPI expression and infiltration of 28 immune cell subsets within the TCGA-LIHC cohort (Fig. 9D and E). Most cell types showed reduced

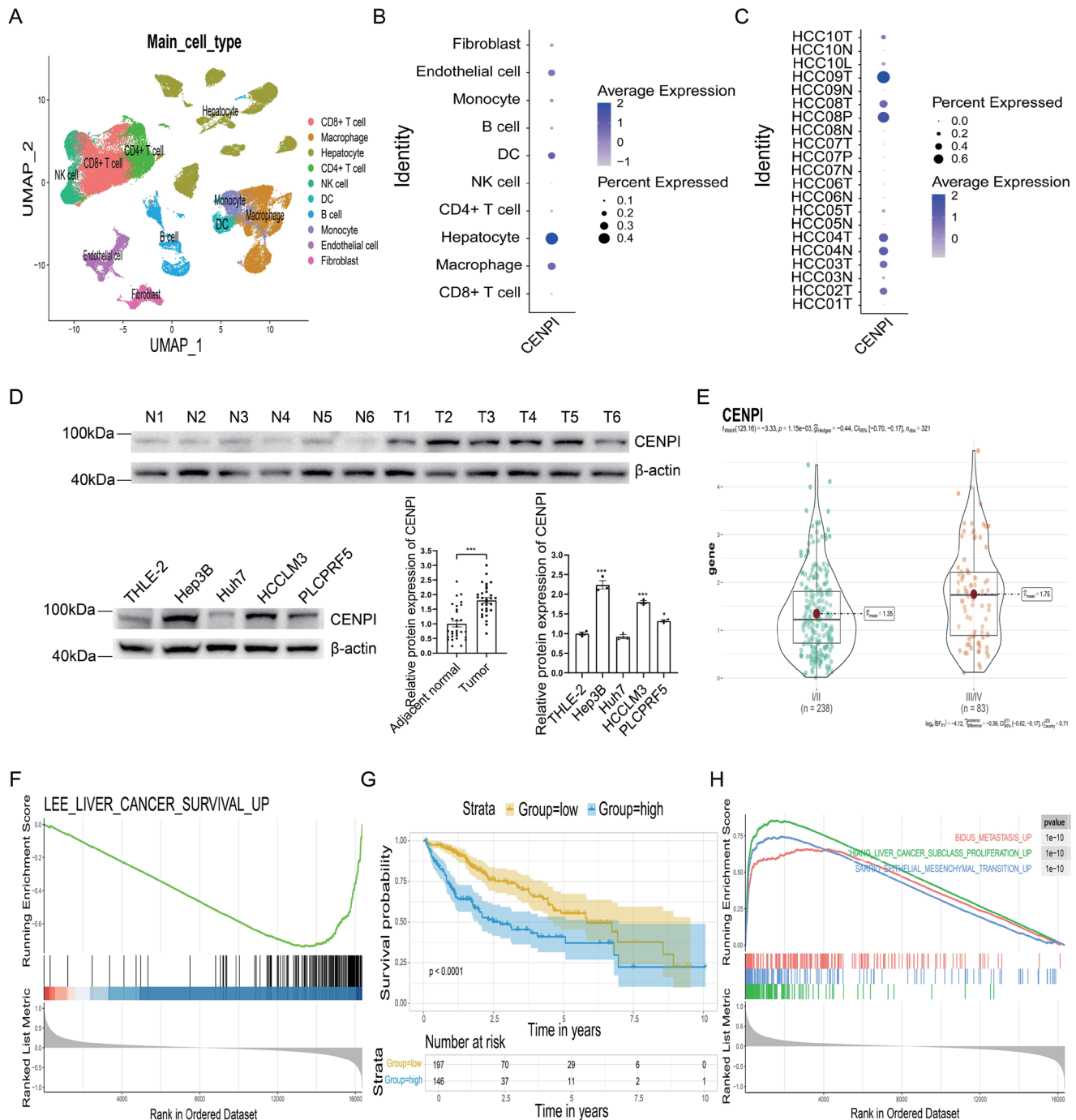


Fig. 5. CENPI expression levels in HCC and associations with unfavorable prognosis. (A) UMAP visualization delineating distinct cellular clusters. (B) Expression patterns of CENPI across various cell types. (C) Expression patterns of CENPI across tissues from different patients. (D) CENPI protein expression in HCC tissues and cell lines. (E) Correlation between CENPI expression level and disease stage in patients. (F, G) The correlation between CENPI expression level and patient survival. (H) The correlation between CENPI expression level and malignant biological behavior of HCC. * $p < 0.05$; *** $p < 0.001$. DC, Dendritic cell; HCC, Hepatocellular carcinoma; NK, Natural killer.

infiltration in the high-CENPI group, including monocytes, central memory CD4⁺ T cells, CD56^{dim} NK cells, plasmacytoid DCs, central memory CD8⁺ T cells, immature DCs, NK cells, gamma delta T cells, activated CD8⁺ T cells, effector memory CD8⁺ T cells, type 1 T helper cells, eosinophils, and neutrophils. Given the critical roles of these cells in antitumor im-

munity, these findings suggested that CENPI might promote immune escape in HCC. Furthermore, patients were stratified into high- and low-CENPI expression groups based on their tumor tissue CENPI levels. Immunohistochemical analysis of corresponding paraffin-embedded sections revealed significantly reduced CD8⁺ T cell infiltration in tumors with elevated

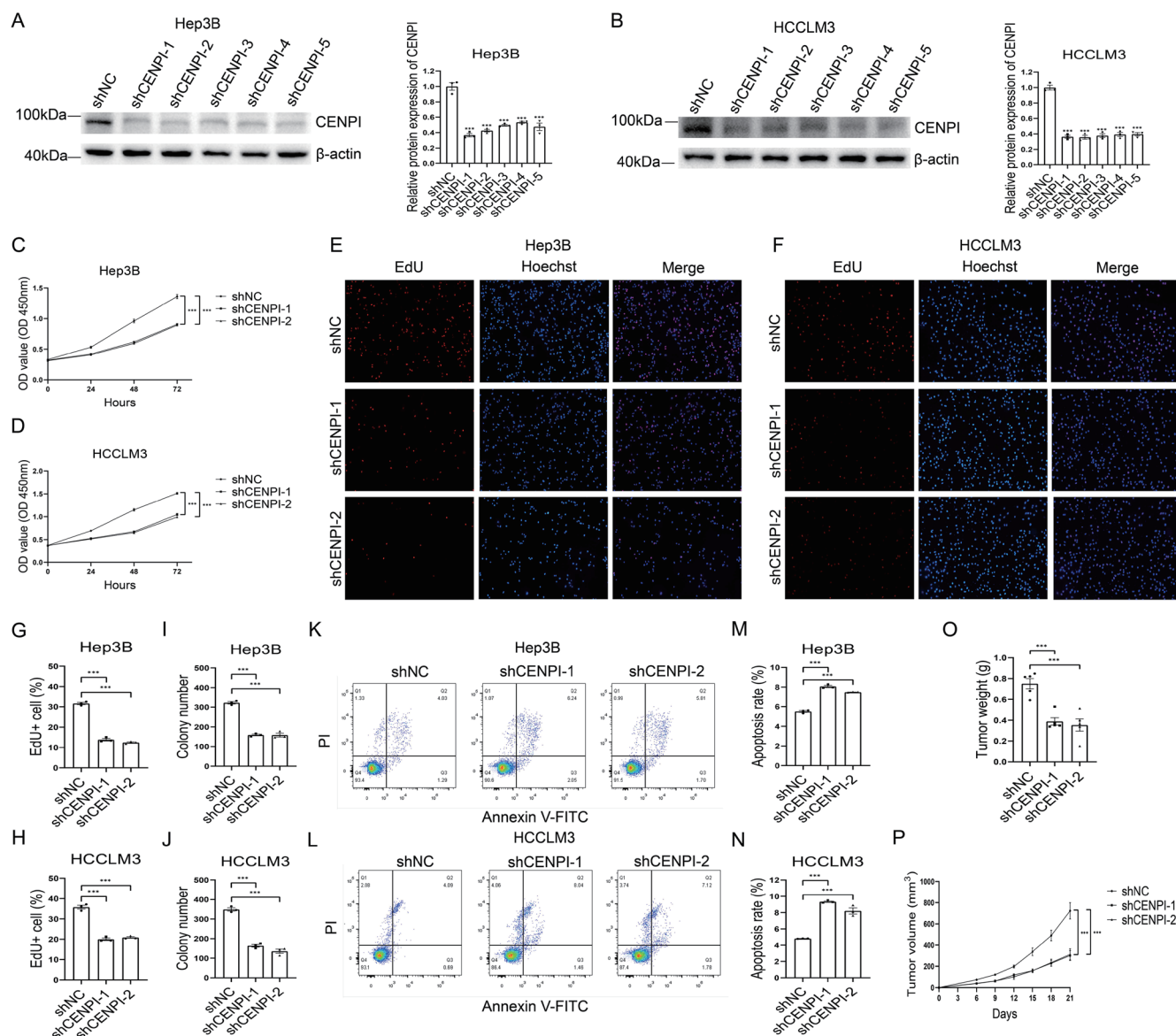


Fig. 6. The effect of CENPI knockdown on proliferation and apoptosis of HCC cells. (A, B) The knockdown efficiency of CENPI protein in Hep3B and HCCLM3 cell lines. (C, D) CCK-8 assay. (E–H) EDU assay. (I, J) Colony formation assay. (K–N) Detection of cell apoptosis using flow cytometry. (O, P) Statistical analysis of tumor weight and volume. *** $p < 0.001$. CCK-8, Cell counting kit-8; EDU, 5-Ethynyl-2'-deoxyuridine; HCC, Hepatocellular carcinoma; OD, Optical density; shNC, short hairpin negative control.

CENPI expression (Fig. 9F). Analysis of immune exhaustion markers and T cell exhaustion status showed that the high-CENPI group exhibited higher levels of exhaustion markers and a greater number of exhausted T cells (Fig. 9G–I). The distribution of exhaustion markers is depicted in Supplementary Figure 5.

CENPI affected cell-to-cell interactions in the TIME

To elucidate the mechanisms of CENPI-mediated immune escape in HCC, we conducted a comprehensive analysis of intercellular communication networks. While no significant differences were observed in the total number of cell-cell interactions between high- and low-CENPI groups, the strength of these interactions was notably diminished in the high-expression cohort (Fig. 10A). Supplementary Figure 6A

and B provide detailed visualizations of intercellular interactions, with line thickness indicating interaction frequency and intensity. We integrated interaction data from both groups to highlight differences, using red to denote stronger interactions in the CENPI-overexpressing group and blue for weaker interactions (Fig. 10B). Figure 10C and Supplementary Figure 6C and D show the activation status of signaling pathways, while Supplementary Figure 6E displays the senders and receivers of cell signals in both groups. Given the pivotal role of MHC-I, CXCL, and CCL signaling pathways in immune cell recruitment, we focused on these pathways. In the high-CENPI group, MHC-I signaling was significantly weaker, indicating that antigen-presenting cells presented tumor antigens to effector cells less frequently. For CXCL signaling, enhanced CD8⁺ T cell recruitment by other cell types was ob-

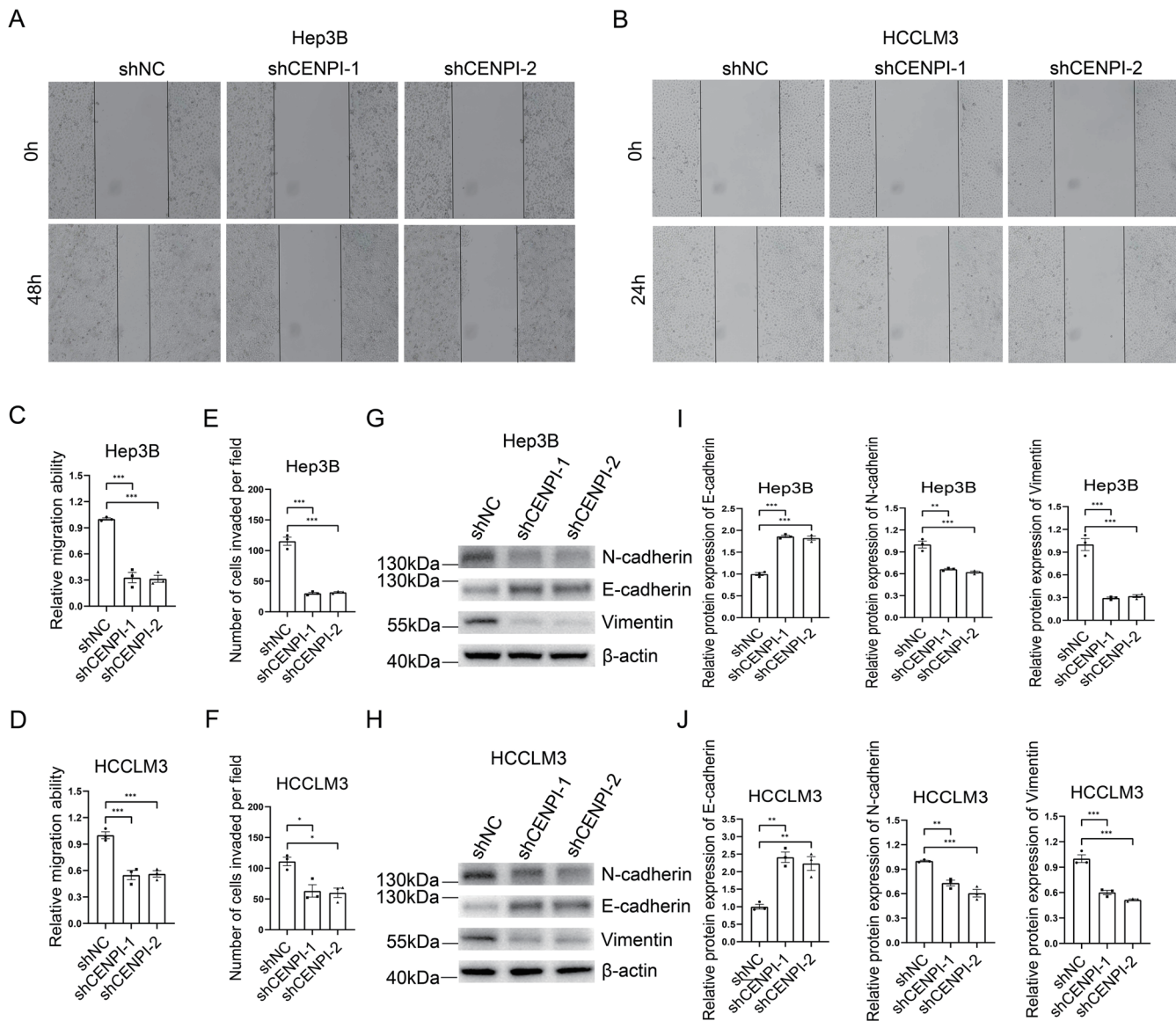


Fig. 7. The effect of CENPI knockdown on migration, invasion, and EMT of HCC cells. (A–D) The wound healing assay. (E, F) The statistical graph of the transwell assay. (G–J) Western blot detection of EMT-related protein expression. * $p < 0.05$; ** $p < 0.01$; *** $p < 0.001$. EMT, Epithelial-mesenchymal transition; HCC, Hepatocellular carcinoma; shNC, short hairpin negative control.

served in the low-CENPI group (Fig. 10D and E). In contrast, CCL signaling analysis revealed no significant differences in effector cell recruitment (Supplementary Fig. 6F). Further analysis of signaling pathway-associated molecules revealed that CENPI knockdown in HCC cells significantly upregulated B2M (a key component of MHC-I) and the chemokines CXCL9 and CXCL10 (Fig. 10F). These findings provide mechanistic insight into CENPI's role in immune escape.

Discussion

In clinical practice, pathological staging remains the cornerstone for predicting long-term survival and guiding treatment decisions in HCC patients. However, due to the inherent heterogeneity of HCC, patients within the same pathological stage often exhibit divergent clinical outcomes, highlighting

the limitations of traditional staging systems for personalized prognosis and therapy. The advent of next-generation sequencing has revolutionized cancer prognosis prediction,⁴² with an increasing number of mRNA- and non-coding RNA-based prognostic biomarkers being developed to forecast patient survival outcomes.^{43,44} CCCs play a critical role in maintaining genomic stability by ensuring accurate DNA replication and proper chromosome segregation during eukaryotic cell division. Within the various stages of the cell cycle, CCCs include DNA damage response checkpoints, DNA replication stress response checkpoints, and mitotic checkpoints. Dysregulation of CCCs at any of these stages can disrupt genetic material transmission, potentially leading to uncontrolled cell proliferation or cell death.⁴⁵ In this study, we systematically analyzed mRNA expression profiles of 292 CCCs in HCC. We subsequently developed and rigorous-

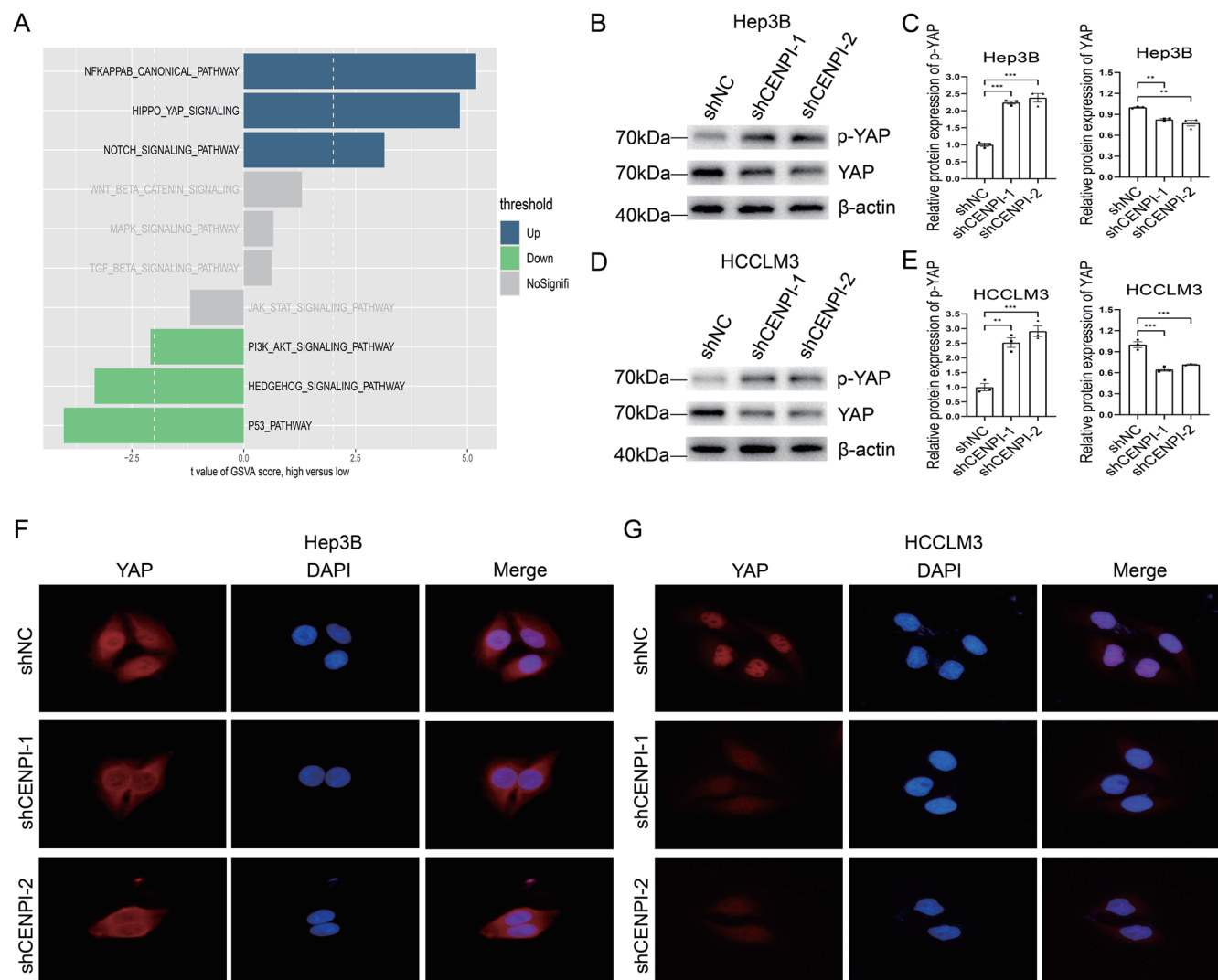


Fig. 8. The effect of CENPI knockdown on the Hippo signaling pathway in HCC cells. (A) GSEA analysis. (B–E) Western blot detection of p-YAP and YAP expression. (F, G) Immunofluorescence detection of YAP localization. ** $p < 0.01$; *** $p < 0.001$. DAPI, 4',6-diamidino-2-phenylindole; GSEA, Gene set variation analysis; HCC, Hepatocellular carcinoma; shNC, short hairpin negative control.

ly validated a prognostic model incorporating 22 CCRGs. Comprehensive evaluation demonstrated that this model effectively predicts OS in HCC patients, providing valuable insights to inform personalized treatment strategies. This approach addresses the limitations of conventional staging systems by capturing molecular heterogeneity within HCC, offering a more precise tool for clinical decision-making and patient stratification.

Over the past decades, accumulating evidence has highlighted the critical role of the CENP family in regulating cancer initiation and progression.^{46–48} Among its members, CENPI exhibits aberrant expression across multiple malignancies. For example, studies have demonstrated its upregulation in gastric cancer, where it promotes tumor proliferation and migration.⁴⁹ Similarly, elevated CENPI expression in lung adenocarcinoma (LUAD) has been shown to drive tumor growth while suppressing apoptosis, with the added finding that CENPI modulates immune cell infiltration in the LUAD tumor microenvironment, a previously unreported observation.²⁶ Despite these insights, the precise functions of CENPI in HCC

remain poorly characterized. In this study, we addressed this knowledge gap through a comprehensive investigation combining multi-omics analysis of TCGA-LIHC and GSE149614 datasets with extensive *in vitro* and *in vivo* experimental validation. Our findings provide novel mechanistic insights into CENPI's role in HCC pathogenesis and tumor immune regulation, establishing a foundation for future therapeutic targeting strategies.

Initially, we observed significantly elevated CENPI protein expression in both HCC tumor tissues and cell lines compared to normal controls. Subsequent functional experiments demonstrated that CENPI knockdown markedly suppressed malignant phenotypes, including reduced tumor cell proliferation, migration, invasion, and EMT, while simultaneously enhancing apoptotic susceptibility. Mechanistically, CENPI facilitated the malignant biological behaviors of HCC by regulating the Hippo pathway. Given that immunotherapy has emerged as a vital treatment modality for HCC,^{11,50} and the well-established influence of the TIME on therapeutic response and clinical outcomes, we further investigated the ef-

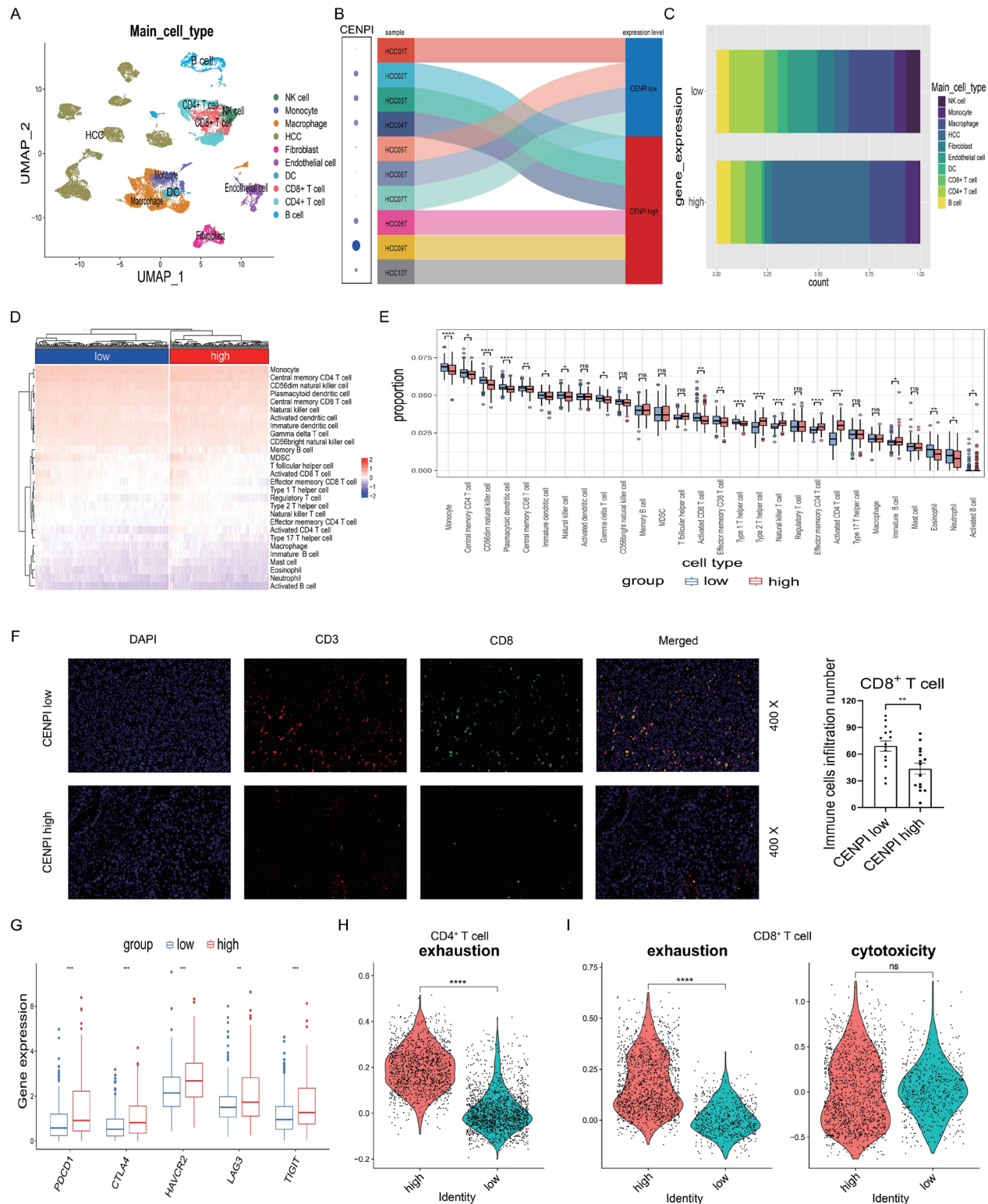
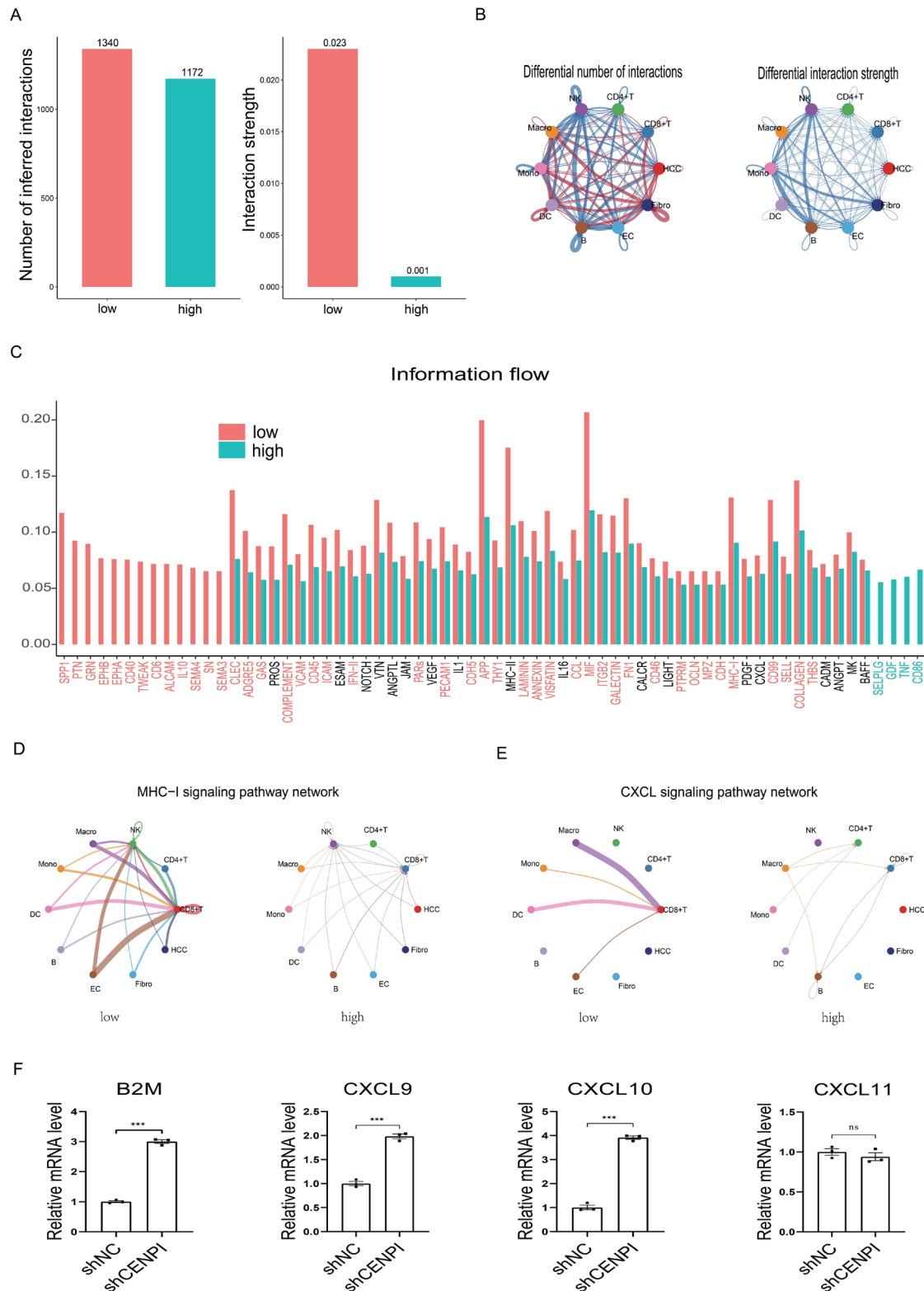


Fig. 9. The influence of CENPI on the immune microenvironment in HCC. (A) UMAP visualization delineating distinct cellular clusters in HCC tissue. (B) Patients grouped according to CENPI expression in HCC cells. (C) The proportion of each cell type within the tumor tissues of the two groups. (D, E) Infiltration levels of 28 immune cell subtypes in the two groups. (F) Immunofluorescence staining of CD8⁺ T cells in tumor tissue sections from patients stratified by CENPI expression (low vs. high). (G) Expression of exhaustion markers in the two groups. (H, I) The status of CD4⁺ T cells and CD8⁺ T cells in the two groups. * $p < 0.05$; ** $p < 0.01$; *** $p < 0.001$; **** $p < 0.0001$. DAPI, 4',6-diamidino-2-phenylindole; DC, Dendritic cell; HCC, Hepatocellular carcinoma; MDSC, Myeloid-derived suppressor cell; NK, Natural killer; UMAP, Uniform manifold approximation and projection.



fects of CENPI on the infiltration and exhaustion status of immune cells within HCC tumor tissue. Patients with high CENPI expression frequently exhibited reduced presence of immune effector cells, such as effector CD8⁺ T cells and NK cells, within their tumors. Moreover, these immune cells were often in a more advanced state of exhaustion, suggesting that elevated CENPI expression may contribute to immune evasion by weakening antitumor immune responses. The underlying mechanisms appear to involve two key processes: (1) impaired antigen presentation by antigen-presenting cells in CENPI-high tumors and (2) diminished chemokine-mediated recruitment of CD8⁺ T cells to the tumor site. Nevertheless, further in-depth research and experimental validation are required. These findings partially align with observations in LUAD, where high CENPI expression was associated with decreased CD8⁺ T cell and NKT cell infiltration, coupled with increased myeloid-derived suppressor cell accumulation. Collectively, our results and existing literature indicate that CENPI functions as an oncogenic driver across multiple malignancies by fostering an immunosuppressive tumor microenvironment that hinders effective immune surveillance and clearance of cancer cells. These insights position CENPI as a potential therapeutic target for reversing immune suppression and enhancing immunotherapy efficacy in HCC.

Conclusions

This study presents a comprehensive investigation into the prognostic significance of CCCRGs in HCC. Notably, our research provides the first mechanistic evidence that CENPI promotes HCC malignant progression through dysregulation of the Hippo pathway, while also revealing its novel role in mediating immune evasion by inhibiting the recruitment of antitumor effector cells, including CD8⁺ T cells and NK cells, to the tumor microenvironment. Although our findings establish a correlation between CENPI overexpression and impaired immune cell infiltration in HCC, the precise molecular mechanisms underlying CENPI-driven immune suppression remain to be fully elucidated. Future studies should focus on dissecting the upstream regulators of CENPI expression, its interactions with immune checkpoint pathways, and its potential role in shaping the tumor immune landscape through metabolic reprogramming or cytokine modulation. Given its dual role in promoting tumor aggressiveness and facilitating immune escape, CENPI represents a promising therapeutic target for HCC treatment. Strategies targeting CENPI, either directly through gene silencing or indirectly via modulation of its regulatory networks, may offer a novel approach to simultaneously inhibit tumor growth and enhance antitumor immunity, potentially improving clinical outcomes for HCC patients.

Acknowledgments

We are grateful to the researchers who built the public databases and to those who shared The Cancer Genome Atlas-Liver Hepatocellular Carcinoma, International Cancer Genome Consortium-Liver Cancer-Riken-Japan, and GSE149614 datasets, which made our study possible through their generous contributions.

Funding

This research was funded by the National Natural Science Foundation of China (Grant Nos. 82472743 and 82300921); the Key R&D Program of Heilongjiang Province (Grant No. GZ2024023); the Natural Science Foundation of Heilongjiang

Province (Grant No. LH2023H043); and the Open Funds of the State Key Laboratory of Oncology in South China (Grant No. HN2025-02).

Conflict of interest

The authors have no conflict of interests related to this publication.

Author contributions

Study concept and design (RH, YX), acquisition of data (RH, YX), analysis and interpretation of data (RH, YX, PZ, LY), drafting of the manuscript (RH, YX), critical revision of the manuscript for important intellectual content (JM, YC), and study supervision (JM, YC). All authors have made significant contributions to this study and have approved the final manuscript.

Ethical statement

The studies involving human participants were reviewed and approved by the Ethics Committee of the Second Affiliated Hospital of Harbin Medical University (YJSKY2023-148), and were conducted in accordance with the Declaration of Helsinki as revised in 2024. The patients/participants provided their written informed consent to participate in this study. The animal experiments received ethical clearance from the Ethics Committee of the Second Affiliated Hospital of Harbin Medical University (YJSDW2023-067), and all procedures complied with the relevant guidelines for animal experimentation. All animals received human care.

Data sharing statement

The datasets used and/or analyzed during the current study are available from the corresponding author upon reasonable request. The data that support the results of the current study are available on The Cancer Genome Atlas (<https://portal.gdc.cancer.gov/>), International Cancer Genome Consortium (<https://dcc.icgc.org/>), and Gene Expression Omnibus websites (<http://www.ncbi.nlm.nih.gov/geo>).

References

- [1] Llovet JM, Kelley RK, Villanueva A, Singal AG, Pikarsky E, Roayaie S, *et al*. Hepatocellular carcinoma. *Nat Rev Dis Primers* 2021;7(1):6. doi:10.1038/s41572-020-00240-3, PMID:33479224.
- [2] Zhang CH, Cheng Y, Zhang S, Fan J, Gao Q. Changing epidemiology of hepatocellular carcinoma in Asia. *Liver Int* 2022;42(9):2029–2041. doi:10.1111/liv.15251, PMID:35319165.
- [3] Anwanwan D, Singh SK, Singh S, Saikam V, Singh R. Challenges in liver cancer and possible treatment approaches. *Biochim Biophys Acta Rev Cancer* 2020;1873(1):188314. doi:10.1016/j.bbcan.2019.188314, PMID:31682895.
- [4] Kudo M, Ueshima K, Ikeda M, Torimura T, Tanabe N, Aikata H, *et al*. Randomised, multicentre prospective trial of transarterial chemoembolisation (TACE) plus sorafenib as compared with TACE alone in patients with hepatocellular carcinoma: TACTICS trial. *Gut* 2020;69(8):1492–1501. doi:10.1136/gutjnl-2019-318934, PMID:31801872.
- [5] Cheng AL, Hsu C, Chan SL, Choo SP, Kudo M. Challenges of combination therapy with immune checkpoint inhibitors for hepatocellular carcinoma. *J Hepatol* 2020;72(2):307–319. doi:10.1016/j.jhep.2019.09.025, PMID:31954494.
- [6] Frendo-Cumbo S, Li T, Ammendolia DA, Coyaude E, Laurent EMN, Liu Y, *et al*. DCAF7 regulates cell proliferation through IRS1-FOXO1 signaling. *iScience* 2022;25(10):105188. doi:10.1016/j.isci.2022.105188, PMID:36248734.
- [7] Liu T, Lin YH, Leng W, Jung SY, Zhang H, Deng M, *et al*. A divergent role of the SIRT1-TopBP1 axis in regulating metabolic checkpoint and DNA damage checkpoint. *Mol Cell* 2014;56(5):681–695. doi:10.1016/j.molcel.2014.10.007, PMID:25454945.
- [8] Matthews HK, Bertoli C, de Bruin RAM. Cell cycle control in cancer. *Nat Rev Mol Cell Biol* 2022;23(1):74–88. doi:10.1038/s41580-021-00404-3, PMID:34508254.
- [9] Neizer-Ashun F, Bhattacharya R. Reality CHECK: Understanding the biol-

- ogy and clinical potential of CHK1. *Cancer Lett* 2021;497:202–211. doi:10.1016/j.canlet.2020.09.016, PMID:32991949.
- [10] Liao J, Chen Z, Chang R, Yuan T, Li G, Zhu C, *et al*. CENPA functions as a transcriptional regulator to promote hepatocellular carcinoma progression via cooperating with YY1. *Int J Biol Sci* 2023;19(16):5218–5232. doi:10.7150/ijbs.85656, PMID:37928273.
- [11] Wei H, Dong C, Li X. Treatment Options for Hepatocellular Carcinoma Using Immunotherapy: Present and Future. *J Clin Transl Hepatol* 2024;12(4):389–405. doi:10.14218/JCTH.2023.00462, PMID:38638377.
- [12] Liu Y, Xun Z, Ma K, Liang S, Li X, Zhou S, *et al*. Identification of a tumour immune barrier in the HCC microenvironment that determines the efficacy of immunotherapy. *J Hepatol* 2023;78(4):770–782. doi:10.1016/j.jhep.2023.01.011, PMID:36708811.
- [13] Langfelder P, Horvath S. WGCNA: an R package for weighted correlation network analysis. *BMC Bioinformatics* 2008;9:559. doi:10.1186/1471-2105-9-559, PMID:19114008.
- [14] Maksimov MO, Pan SJ, James Link A. Lasso peptides: structure, function, biosynthesis, and engineering. *Nat Prod Rep* 2012;29(9):996–1006. doi:10.1039/c2np20070h, PMID:2283149.
- [15] Guo L, Wang Z, Du Y, Mao J, Zhang J, Yu Z, *et al*. Random-forest algorithm based biomarkers in predicting prognosis in the patients with hepatocellular carcinoma. *Cancer Cell Int* 2020;20:251. doi:10.1186/s12935-020-01274-z, PMID:32565735.
- [16] Skelin M, Perkovic-Stipić B, Lucijanić M, Javor E, Krečak I. Survival analysis of diabetes cardiovascular outcome trials using reconstructed Kaplan-Meier curves. *Eur J Intern Med* 2024;128:153–155. doi:10.1016/j.ejim.2024.05.026, PMID:38797637.
- [17] Wang Q, Qiao W, Zhang H, Liu B, Li J, Zang C, *et al*. Nomogram established on account of Lasso-Cox regression for predicting recurrence in patients with early-stage hepatocellular carcinoma. *Front Immunol* 2022;13:1019638. doi:10.3389/fimmu.2022.1019638, PMID:36505501.
- [18] Cui Y, Zhou X, Zhang J, Fang B, Ge J, Tang H, *et al*. Exploiting potential molecular compounds for treating testicular seminoma by targeting immune related genes. *Cell Commun Signal* 2024;22(1):560. doi:10.1186/s12964-024-01927-w, PMID:39574183.
- [19] Huang Y, Luo W, Chen S, Su H, Zhu W, Wei Y, *et al*. Association of a Novel DOK2 Mutation-Related Gene Signature With Immune in Hepatocellular Carcinoma. *Front Genet* 2022;13:872224. doi:10.3389/fgene.2022.872224, PMID:35620462.
- [20] Yoshihara K, Shahmoradgol M, Martínez E, Vegesna R, Kim H, Torres-García W, *et al*. Inferring tumour purity and stromal and immune cell admixture from expression data. *Nat Commun* 2013;4:2612. doi:10.1038/ncomms3612, PMID:24113773.
- [21] Yu B, Yin YX, Tang YP, Wei KL, Pan ZG, Li KZ, *et al*. Diagnostic and Predictive Value of Immune-Related Genes in Crohn's Disease. *Front Immunol* 2021;12:643036. doi:10.3389/fimmu.2021.643036, PMID:33936061.
- [22] Mayakonda A, Lin DC, Assenov V, Plass C, Koeffler HP. Maftools: efficient and comprehensive analysis of somatic variants in cancer. *Genome Res* 2018;28(11):1747–1756. doi:10.1101/gr.239244.118, PMID:30341162.
- [23] Lu Y, Yang A, Quan C, Pan Y, Zhang H, Li Y, *et al*. A single-cell atlas of the multicellular ecosystem of primary and metastatic hepatocellular carcinoma. *Nat Commun* 2022;13(1):4594. doi:10.1038/s41467-022-32283-3, PMID:35933472.
- [24] Jin S, Guerrero-Juarez CF, Zhang L, Chang I, Ramos R, Kuan CH, *et al*. Inference and analysis of cell-cell communication using CellChat. *Nat Commun* 2021;12(1):1088. doi:10.1038/s41467-021-21246-9, PMID:33597522.
- [25] Wang C, Liao Y, He W, Zhang H, Zuo D, Liu W, *et al*. Elafin promotes tumour metastasis and attenuates the anti-metastatic effects of erlotinib via binding to EGFR in hepatocellular carcinoma. *J Exp Clin Cancer Res* 2021;40(1):113. doi:10.1186/s13046-021-01904-y, PMID:33771199.
- [26] Feng Z, Cui G, Tan J, Liu P, Chen Y, Jiang Z, *et al*. Immune infiltration related CENPI associates with the malignant features and drug resistance of lung adenocarcinoma. *Biochim Biophys Acta Mol Basis Dis* 2024;1870(3):167017. doi:10.1016/j.bbdis.2024.167017, PMID:38232915.
- [27] Zhang Z, Chen X, Li Y, Zhang F, Quan Z, Wang Z, *et al*. The resistance to anoikis, mediated by Spp1, and the evasion of immune surveillance facilitate the invasion and metastasis of hepatocellular carcinoma. *Apoptosis* 2024;29(9–10):1564–1583. doi:10.1007/s10495-024-01994-x, PMID:39066845.
- [28] Li Y, Yang X, Geng C, Liu Y, Tang T, Zhang L, *et al*. Identification of molecular subtypes based on chromatin regulator-related genes and experimental verification of the role of ASCL1 in conferring chemotherapy resistance to breast cancer. *Front Immunol* 2024;15:1390261. doi:10.3389/fimmu.2024.1390261, PMID:38726001.
- [29] Tian Z, Xu C, He W, Lin Z, Zhang W, Tao K, *et al*. The deubiquitinating enzyme USP19 facilitates hepatocellular carcinoma progression through stabilizing YAP. *Cancer Lett* 2023;577:216439. doi:10.1016/j.canlet.2023.216439, PMID:37832781.
- [30] Wang J, Yu H, Dong W, Zhang C, Hu M, Ma W, *et al*. N6-Methyladenosine-Mediated Up-Regulation of FZD10 Regulates Liver Cancer Stem Cells' Properties and Lenvatinib Resistance Through WNT/β-Catenin and Hippo Signaling Pathways. *Gastroenterology* 2023;164(6):990–1005. doi:10.1053/j.gastro.2023.01.041, PMID:36764493.
- [31] Wang W, Zhang Y, Huang X, Li D, Lin Q, Zhuang H, *et al*. The role of the miR-30a-5p/BCL2L1 pathway in rosmarinic acid-induced apoptosis in MDA-MB-231-derived breast cancer stem-like cells. *Front Pharmacol* 2024;15:1445034. doi:10.3389/fphar.2024.1445034, PMID:39239646.
- [32] Li S, Zhang Z, Li Z, Yang L, Liu J, Liu Y, *et al*. CENPA promotes glutamine metabolism and tumor progression by up-regulating SLC38A1 in endometrial cancer. *Cell Signal* 2024;117:111110. doi:10.1016/j.cellsig.2024.111110, PMID:38382691.
- [33] Wu G, Fan Z, Li X. CENPA knockdown restrains cell progression and tumor growth in breast cancer by reducing PLA2R1 promoter methylation and modulating PLA2R1/HHEX axis. *Cell Mol Life Sci* 2024;81(1):27. doi:10.1007/s00018-023-05063-5, PMID:38212546.
- [34] Huang Z, Zhou JK, Wang K, Chen H, Qin S, Liu J, *et al*. PDLIM1 Inhibits Tumor Metastasis Through Activating Hippo Signaling in Hepatocellular Carcinoma. *Hepatology* 2020;71(5):1643–1659. doi:10.1002/hep.30930, PMID:31509262.
- [35] Wang Q, Zhang C, Pang Y, Cheng M, Wang R, Chen X, *et al*. Comprehensive analysis of bulk, single-cell RNA sequencing, and spatial transcriptomics revealed IER3 for predicting malignant progression and immunotherapy efficacy in glioma. *Cancer Cell Int* 2024;24(1):332. doi:10.1186/s12935-024-03511-1, PMID:39354533.
- [36] Gu Y, Ding C, Yu T, Liu B, Tang W, Wang Z, *et al*. SIRT7 promotes Hippo/YAP activation and cancer cell proliferation in hepatocellular carcinoma via suppressing MST1. *Cancer Sci* 2024;115(4):1209–1223. doi:10.1111/cas.16091, PMID:38288904.
- [37] He R, Guan C, Zhao X, Yu L, Cui Y. Expression of immune related genes and possible regulatory mechanisms in different stages of non-alcoholic fatty liver disease. *Front Immunol* 2024;15:1364442. doi:10.3389/fimmu.2024.1364442, PMID:38524129.
- [38] Nguyen-Lefebvre AT, Selzner N, Wrana JL, Bhat M. The hippo pathway: A master regulator of liver metabolism, regeneration, and disease. *FASEB J* 2021;35(5):e21570. doi:10.1096/fj.202002284RR, PMID:33831275.
- [39] Liu Y, Wang X, Yang Y. Hepatic Hippo signaling inhibits development of hepatocellular carcinoma. *Clin Mol Hepatol* 2020;26(4):742–750. doi:10.3350/cmh.2020.0178, PMID:32981290.
- [40] Li S, Hao L, Li N, Hu X, Yan H, Dai E, *et al*. Targeting the Hippo/YAP1 signaling pathway in hepatocellular carcinoma: From mechanisms to therapeutic drugs (Review). *Int J Oncol* 2024;65(3):88. doi:10.3892/ijo.2024.5676, PMID:39092548.
- [41] Yuan T, Zhou T, Qian M, Du J, Liu Y, Wang J, *et al*. SDHA/B reduction promotes hepatocellular carcinoma by facilitating the deNEDDylation of cullin1 and stabilizing YAP/TAZ. *Hepatology* 2023;78(1):103–119. doi:10.1002/hep.32621, PMID:35713976.
- [42] Nair M, Sandhu SS, Sharma AK. Cancer molecular markers: A guide to cancer detection and management. *Semin Cancer Biol* 2018;52(Pt 1):39–55. doi:10.1016/j.semcancer.2018.02.002, PMID:29428478.
- [43] Liang JY, Wang DS, Lin HC, Chen XX, Yang H, Zheng Y, *et al*. A Novel Ferroptosis-related Gene Signature for Overall Survival Prediction in Patients with Hepatocellular Carcinoma. *Int J Biol Sci* 2020;16(13):2430–2441. doi:10.7150/ijbs.45050, PMID:32760210.
- [44] Yang S, Ji J, Wang M, Nie J, Wang S. Construction of Ovarian Cancer Prognostic Model Based on the Investigation of Ferroptosis-Related lncRNA. *Biomolecules* 2023;13(2):306. doi:10.3390/biom13020306, PMID:36830675.
- [45] Wang H, Wang W, Wang Z, Li X. Transcriptomic correlates of cell cycle checkpoints with distinct prognosis, molecular characteristics, immunological regulation, and therapeutic response in colorectal adenocarcinoma. *Front Immunol* 2023;14:1291859. doi:10.3389/fimmu.2023.1291859, PMID:38143740.
- [46] Qi CL, Huang ML, Zou Y, Yang R, Jiang Y, Sheng JF, *et al*. The IRF2/CENP-N/AKT signaling axis promotes proliferation, cell cycling and apoptosis resistance in nasopharyngeal carcinoma cells by increasing aerobic glycolysis. *J Exp Clin Cancer Res* 2021;40(1):390. doi:10.1186/s13046-021-02191-3, PMID:34893086.
- [47] Tucker JB, Carlsen CL, Scribano CM, Pattaswamy SM, Burkard ME, Weaver BA. CENP-E Inhibition Induces Chromosomal Instability and Synergizes with Diverse Microtubule-Targeting Agents in Breast Cancer. *Cancer Res* 2024;84(16):2674–2689. doi:10.1158/0008-5472.CAN-23-3332, PMID:38832939.
- [48] Feng Z, Chen Y, Cai C, Tan J, Liu P, Chen Y, *et al*. Pan-Cancer and Single-Cell Analysis Reveals CENPL as a Cancer Prognosis and Immune Infiltration-Related Biomarker. *Front Immunol* 2022;13:916594. doi:10.3389/fimmu.2022.916594, PMID:35844598.
- [49] Wang J, Liu X, Chu HJ, Li N, Huang LY, Chen J. Centromere Protein I (CENP-I) Is Upregulated in Gastric Cancer, Predicts Poor Prognosis, and Promotes Tumor Cell Proliferation and Migration. *Technol Cancer Res Treat* 2021;20:15330338211045510. doi:10.1177/15330338211045510, PMID:34617858.
- [50] Llovet JM, Castet F, Heikenwalder M, Maini MK, Mazzaferro V, Pinato DJ, *et al*. Immunotherapies for hepatocellular carcinoma. *Nat Rev Clin Oncol* 2022;19(3):151–172. doi:10.1038/s41571-021-00573-2, PMID:34764464.